Published in final edited form as:
J Mater Chem B Mater Biol Med. 2013 June 14; 1(22): 2807–2817. doi:10.1039/C3TB20256A.

Synthesis, Stability, Cellular Uptake, and Blood Circulation Time of Carboxymethyl-Inulin Coated Magnetic Nanoparticles

Lenibel Santiago-Rodríguez[a], **Moises Montalvo Lafontaine**[a], **Cristina Castro**[b], **Janet Méndez-Vega**[a], **Magda Latorre-Esteves**[a], **Eduardo J. Juan**[c], **Edna Mora**[b], **Madeline Torres-Lugo**[a], and **Carlos Rinaldi**[d,e]

Cristina Castro: carlos.rinaldi@bme.ufl.edu

[a]Department of Chemical Engineering, University of Puerto Rico, Mayagüez Campus, P.O. Box 9000, Mayagüez PR 00681, Puerto Rico

[b]Puerto Rico Cancer Center, University of Puerto Rico, Medical Sciences, P.O. Box 365067, San Juan PR 00936-5067, Puerto Rico

[c]Department of Electrical and Computer Engineering, University of Puerto Rico, Mayagüez Campus, P.O. Box 9000, Mayagüez PR 00681, Puerto Rico

[d]J. Crayton Pruitt Family Department of Biomedical Engineering, University of Florida, P.O. Box 116131, Gainesville, FL, USA, Fax: +1 352 273 9221; Tel: +1 352 294 5588

[e]Department of Chemical Engineering, University of Florida, P.O. Box 116131, Gainesville, FL, USA

Abstract

Iron oxide nanoparticles were coated with the biocompatible, biodegradable, non-immunogenic polysaccharide inulin by introduction of carboxyl groups into the inulin structure and conjugation with amine groups on the surface of iron oxide nanoparticles grafted with 3-aminopropyltriethoxysilane. The resulting nanoparticles were characterized by FT-IR spectroscopy, transmission electron microscopy, dynamic light scattering, zeta potential, SQUID magnetometry, and with respect to their energy dissipation rate in applied alternating magnetic fields. The nanoparticles had a hydrodynamic diameter in the range of 70 ± 10 nm and were superparamagnetic, with energy dissipation rates in the range of 58–175 W/g for an applied field frequency of 233 kHz and an applied field amplitude in the range of 20–48 kA/m. The nanoparticles were stable in a range of pH, at temperatures between 23°C and 53°C, and in short term storage in water, PBS, and culture media. The particles were non-cytotoxic to the immortalized human cancer cell lines Hey A8 FDR, A2780, MDA 468, MCF-7 and Caco-2. The nanoparticles were readily taken up by Caco-2 cells in a time and concentration dependent fashion, and were found to have a pharmacokinetic time constant of 47 ± 3 min. The small size, non-cytotoxicity, and efficient energy dissipation of the particles could make them useful for biomedical applications such as magnetic fluid hyperthermia.

Introduction

Iron oxide nanoparticles (IO-NPs), mainly magnetite (Fe_3O_4) and maghemite (γFe_2O_3),[1] are attractive in many applications because they can be manipulated using external magnetic fields, they are believed to be biocompatible, and there are many methods to synthesize and modify them chemically. These field-responsive nanomaterials have promise in applications such as biosensors, drug delivery, nanoscale hyperthermia, and magnetic resonance imaging.[1–4]

In many of their potential biomedical applications IO-NPs would be delivered intravenously and targeted to intended tissues either passively, through the enhanced permeation and retention effect, or actively, using a targeting agent. Unfortunately, bare IO-NPs possess poor stability in aqueous solutions due to van der Waals and magnetic attraction and their large surface-to-volume ratio.[5] This results in IO-NP aggregation to sizes above 100 nm, which would be rapidly removed from the blood stream via the reticuloendothelial system.[6] To overcome this limitation, researchers have modified IO-NPs with a wide variety of compounds, such as polyethylene glycol, polyanhydrides, poly (lactic acid), and poly (vinyl alcohol) (PVA), among others.[5] Unfortunately, many of these surface coatings suffer disadvantages such as causing an immunogenic response, promoting non-specific uptake, producing toxic degradation products, or promoting adsorption of plasma proteins leading to loss of colloidal stability.[7, 8]

Among the many types of coatings used, polysaccharides have demonstrated to be good IO-NPs stabilizers.[9] One of the most often used polysaccharide for this purpose is dextran. In fact, IO-NPs coated with dextran are commercially and clinically available under the trademarks Ferridex, Resovist, and Sinerem.[10] Although dextran coatings have shown promise in many applications, dextran can be easily degraded by enzymes called dextranases and may interfere with the normal blood clotting process.[11, 12] Thus, IO-NPs coated with dextran may rapidly degrade *in vitro* and *in vivo* and their interaction with other blood components may result in changes in their surface chemistry and their non-specific accumulation in unintended sites.

Here we propose the use of inulin as a biocompatible stabilizing coating for IO-NPs. Inulin is a polysaccharide that consists of repeat units of fructose that has found application in the food and pharmaceutical industries.[13] Contrary to dextran, which consists of glucose repeat units, inulin is exogenous to the human body. It is mainly encountered in plants and vegetables, such as onions, garlic, and chicory.[14] Inulin is biocompatible, readily available, is easy to modify chemically and there are no native enzymes in the human body that can degrade it.[15] Inulin is degraded in the colon due to the presence of bifidobacteria that can decompose it into carbon dioxide and short chain fatty acids, such as butyric and propionic acids that are believed to inhibit colon cancer growth.[16] Furthermore, inulin is injected intravenously to measure glomerular blood filtration rate.[17] Inulin is useful for this purpose because it has low non-specific absorption in most tissues and is easily filtered by the kidneys. The above properties and medical uses of inulin suggest that this polysaccharide may be valuable in obtaining colloidally stable IO-NPs suitable for biomedical applications.

Herein we describe a route to obtain IO-NPs coated with inulin. We first carboxymethylate inulin to add carboxylic acid moeities.[18] The product of that reaction, carboxymethyl-inulin (CMI), has been found to be safe for humans.[19] IO-NPs are then coated with 3-aminopropyltriethoxysilane (APS), providing an amine group that can readily form amide bonds with the carboxymethyl group of the modified inulin. These iron oxide nanoparticles conjugated with carboxymethyl-inulin (IO-CMI) were characterized using various chemical, physical, and magnetic methods. Colloidal stability was investigated under a variety of conditions in aqueous and in cell culture media. Cytotoxicity and cellular uptake were investigated *in vitro* and blood circulation time was determined *in vivo*.

Experimental

Iron (II) chloride tetrahydrate ($FeCl_2 \cdot 4H_2O$, 99%), iron (III) chloride hexahydrate ($FeCl_3 \cdot 6H_2O$, 97%), ammonium hydroxide (NH_4OH, 29% v/v), inulin from dahlia tubers, chloroacetic acid (≥99.0%), 1-Ethyl-3-(3-dimethylaminopropyl)carbodiimide hydrochloride (EDC), *N*-hydroxysuccinimide (NHS), tetramethylammonium 29%, dimethyl sulfoxide

(DMSO, 99.9%), Hank's balanced salt solution (HBSS), phosphate buffer saline (PBS), trypsin-EDTA solution (0.25%), amphotericin B solution, penicillin-streptomycin solution, Gentamicin, Dulbecco's modified eagle's medium (DMEM) and RPMI-1640 media were purchased from Sigma Aldrich. Minimum essential medium (EMEM) was purshased from SAFC Biosciences. Fetal bovine serum (FBS) was obtained from Invitrogen. 3-aminopropyltriethoxysilane (APS) was purchased from TCI America. Sodium hydroxide (ACS reagent) and nitric acid (Optima grade, 68–70%) were purchased from Fisher Scientific. Sodium chloride (99.5%) were purchased from Acros Organics. CellTiter-Blue™ was obtained from Promega. MCF-7 and Caco-2 cells lines were purchased from ATCC©. Hey A8 FDR, A2780 and MDA 468 were donated by the University of Texas MD Anderson Cancer Center. All chemicals were used as received. Aqueous solutions were prepared using nanopure water (18.2 MΩ-cm)

Synthesis and modification of iron oxide nanoparticles with APS

Iron oxide nanoparticles were synthesized using the co-precipitation method.[20] In summary, a mixture of 1:2 ferrous and ferric chloride salts was diluted in nitrogen-purged water. The solution mixture was constantly purged with nitrogen and heated to 70°C, at which point ammonium hydroxide was added. The temperature of the solution was held at 80°C for an hour under stirring and the pH of the solution was maintained at 8.0 by periodic addition of ammonium hydroxide. Afterwards, the solution was allowed to reach room temperature and then the particles were centrifuged and peptized using tetramethylammonium hydroxide. Approximately 0.1 g of peptized nanoparticles were suspended in 75 ml of DMSO, followed by addition of 10 ml of APS, 0.2 ml of acetic acid, and 1.25 ml of deionized water. This mixture was left to react for 72 hours. The modified nanoparticles were washed using ethanol and separated by magnetic decantation. The final nanoparticle product was left to dry under atmospheric conditions.

Synthesis of carboxymethyl-inulin

Inulin was carboxymethylated using a method described in the literature for cellulose and adapted by our group to synthesize carboxymethyl dextran.[21] Inulin was dissolved in deionized water and a cold solution of NaOH was added for a final concentration of 3.0 M. Chloroacetic acid (1.8 M) was added immediately and the mixture was heated at 60°C for an hour. After the reaction mixture reached room temperature an excess of ethanol was added to precipitate the reaction product overnight. The precipitate was dialyzed against distilled water to remove unreacted reagents and salts. The product was dried in a vacuum oven and is referred to as carboxymethyl-inulin (CMI) hereon.

Attachment of carboxymethyl-inulin to iron oxide nanoparticles

Iron oxide nanoparticles were conjugated to CMI via amide bond formation between the amine groups of APS molecules on the particles and the carboxyl groups of CMI. A suspension of 0.1 mg/mL of IO-APS particles was prepared in deionized water and mixed with a solution of 10 g/mL of CMI, previously activated using 2.5 mg/ml of EDC and 1.5 mg/ml of NHS. The reaction mixture was placed in a shaker for 36 h at 150 rpm. The particles were precipitated using ethanol and magnetically recovered after centrifugation at 8,000 rpm for 10 minutes. The nanoparticles were dried in a vacuum oven and stored in a desiccator until they were used.

Characterization of IO-CMI

Particles were characterized using a FT-IR spectrometer (Varian 800) in a ZnSe attenuated total reflection sample holder. Solid samples were dried at 60°C under vacuum for 24 hours and recorded at a resolution of 8 cm^{-1}. The magnetic properties of the particles were

determined using a superconducting quantum interference device (SQUID) magnetometer (Quantum design MPMS XL-7) at 300 K. The hydrodynamic diameter (D_h) and zeta potential (ζ-potential) of the particles were measured using a particle size and zeta potential analyzer (BI-90 Plus from Brookhaven Instruments). This instrument operates using a He-Ne red laser at a power, scattering angle and wavelength of 35 mW, 90° and 633 nm, respectively. The ζ-potential measurements were obtained in a 1 mM KNO_3 solution. The nanopure water used to prepare the samples for the ζ-potential and D_h measurements was filtered using Whatman™ 0.2 μm Nylon filters. The pH of the solutions was adjusted using 0.1 M KOH and 0.1 M HNO_3. Nanoparticles were characterized using transmission electron microscopy (TEM, Leo 922 200 kV, Carl Zeiss) to determine the size distribution and morphology of the particles. Size distributions were estimated by measuring individual particles using the ImageJ program. Samples were prepared by dispersing nanoparticles at a concentration of 0.01 mg/mL in water. Formvar® carbon-coated copper grids (Ted Pella) were then immersed in the particle suspensions and dried at room temperature. The iron oxide core content of the particles was estimated using a thermogravimmetric analyzer (TGA/DSC 1, Mettler Toledo International Inc.). Cytotoxicity assays were performed using a fluorescence microplate reader (Spectra MAX GeminiEM, Molecular Devices). Specific absorption rate measurements were obtained for 1 mL of 0.6 mg/mL of IO-CMI dispersed in DI water. An RDO Induction HFI 3-135/400 (RDO Enterprises Inc, Washington, NJ) was used to drive an ethylene glycol cooled hollow four-turn induction coil at a radio frequency of 233 kHz was used. The field amplitudes were 20, 37.5 and 47.5 kA/m and were applied for 5 minutes. The increase in temperature was recorded using a fiber-optic thermometer.

Cytotoxicity Assay

Cell viability was estimated through the ability of metabolically active cells to reduce resazurin into resorufin, a fluorescent product excited at 579 nm and measured at 590 nm. MDA-MB-468, MCF-7 and Caco-2 cell lines were seeded in 96-well plates at a density of 1.2×10^4 cells cm^{-2} in DMEM with 10% (v/v) FBS for 48 hours. Then, they were incubated with IO-CMI at 0.1, 0.3, 0.6, 1.5 and 3.5 mg/mL for five days. The nanoparticle solution was removed and the cells were washed with HBSS and replaced with 120 ul of CellTiter-Blue solution. Controls for MDA-MB-468, MCF-7, and Caco-2 cell lines consisted of cells incubated for seven days. The plates were incubated for 2 hours, protected from light, and fluorescence intensity was recorded. For Hey A8 FDR and A2780 cells lines a density of 1.0×10^4 cells cm^{-2} in RPMI with 20% FBS was used and incubated for 24 hours. For these cell lines the incubation time with the different nanoparticle solution concentrations was 48 hours. The nanoparticle solutions were prepared by first sterilizing the IO-CMI powder by autoclave at 121°C for 1 hour, followed by their suspension in the desired culture medium with 10% FBS. Controls for Hey A8 FDR and A2780 cell lines consisted of cells incubated for three days. Because the CMI is attached covalently to the nanoparticles, sterilization by autoclave did not affect the coating or colloidal stability. Cells exposed to 1.5% bleach and to cell culture medium were used as positive and negative controls, respectively. Wells without cells were used to determine the fluorescent background.

Cellular Uptake of IO-CMI nanoparticles

Caco-2 cells were chosen for the study of cellular uptake of IO-CMI nanoparticles. Cells were seeded in 6-well plates at a density of 5×10^5 cell cm^{-2} using EMEM with 10% FBS. The cells were incubated with 0.1 mg/mL of Fe, which corresponds to approximately 0.14 mg/mL of IO-NPs assuming that all the iron measured in the nanoparticle solution is in the form of magnetite (Fe_3O_4), for 1, 6, 12 and 24 hours. The nanoparticle solution was prepared by autoclaving the nanoparticle powder at 121°C for 1 hour. Then, the nanoparticles were suspended in EMEM medium with 10 % FBS. After incubation of the cells with the nanoparticle suspension, cells were washed three times with PBS, detached by

vigorous pipetting, counted in a hematocytometer and centrifuged (Centrific Model 228 from Fisher Scientific) for 10 minutes. The supernatant was discarded and the cell pellet digested in 70 % HNO_3 (Optima Grade, Fisher) for an hour at 101°C using a dry heat block. The acid solution was diluted in deionized water in order to obtain a final solution of 3% HNO_3. The solutions were filtered with PVDF filters with a 0.45 μm pore size before ICP measurements. The ICP instrument was calibrated using iron standard solution from 0.001 to 200 ppb. A 3% HNO_3 solution was used as control. The same procedure was followed for an experiment with IO-CMI nanoparticle concentrations of 0, 0.020, 0.040, 0.060, 0.080 and 0.100 mg/mL of Fe and an incubation time of 24 hours. All the measurements were corrected by subtracting the measured iron content in cells in the control groups.

Pharmacokinetic Study

Animal experiments were conducted under protocols approved by the Institutional Animal Care and Use Committee. Five female Sprague Dawley rats, 3 weeks of age (200 ± 20 g), and cannulated through the jugular vein were obtained from Taconic, Germantown, NY. Clearance of IO-CMI nanoparticles from the blood stream was monitored by injecting animals with a sterile IO-CMI solution and extracting blood samples at pre-selected intervals for subsequent determination of Fe content through a spectrophotometric assay. For each animal, 500 ul of blood was extracted initially and used to determine the baseline Fe content in the blood and to allow delivery of 500 ul of the nanoparticle solution, at a concentration of 5 mg/mL of Fe_3O_4. To ensure complete delivery of the nanoparticle solution the catheter was flushed using 50 ul of saline solution followed by 50 ul of lock-in solution (heparinized glycerol, 500 IU/ml) to prevent blood coagulation in the catheter. Then, 150 ul blood samples were extracted after 10, 20, 40, 60, 80, 100, 120, 240, 360, 480, 720, 1080, and 1440 minutes, each time followed by injection of 50 ul of saline solution and 50 ul of lock-in solution. Blood samples were collected in microtubes with Heparin and sample mass was measured. Then, samples were centrifuged at 4°C and 10,000 rpm for 10 min, and 60 ul of plasma were collected and snap frozen in liquid nitrogen. The plasma samples were weighted and digested for 12 hours in 1 mL of 70% HNO_3 at 101°C. Then, 30 ul of the acid solution was evaporated for an hour at 115°C, followed by addition of 0.6 M of hydroxylamine hydrochloride and reaction for 1 hour in order to reduce the Fe(III) to Fe(II). Iron content was measured by adding 0.3 M sodium citrate and 4.8 mM 1,4-phenanthroline to form a colored iron complex that absorbs at 508 nm.[22] The solutions were measured in a spectrophotometer (UV/Vis-2401 PC, Shimadzu Scientific Instruments, Inc.) and compared to a standard calibration curve.

Results and Discussion

FT-IR Characterization

Inulin (α-D-glucopyranosyl-[β-D-fructofuranosyl](n-1)-D-fructofuranoside), is a linear polysaccharide consisting of fructosyl fructose units (β-1,2) which sometimes include one glucopyranose unit at the chain end. Fig. 1(a) shows the infrared spectra of inulin from Dahlia tuber after drying in a vacuum oven. The spectra exhibit a broad band at 3360 cm^{-1} from the hydroxyl stretching (-OH) of fructose and glucose units.[23, 24] Two bands at around 2925 cm^{-1} were observed accompanied by several bands in the region between 1500 and 1250 cm^{-1} and can be ascribed to stretching and bending modes of the aliphatic groups –CH and $–CH_2$, respectively. The band at 1637 cm^{-1} can be assigned to the hydroxyl bending mode. While the bands below 1600 cm^{-1} are characteristic of the vibrational modes of carbohydrates.[25] The bands between 1440 and 1353 cm^{-1} originate from the combination of –OCH and –COH deformation modes.[24, 25] More specifically, the region between 1354 and 1191 cm^{-1} can be designated to –CH and –OH deformations.[25] Bands in the region between 1200 and 1000 cm^{-1} are commonly found in carbohydrates and are assigned to C-O, C-O-C,

C-C-C, and C-CO antisymmetric stretches. The bands around 1000 cm^{-1} are associated with –C-O stretching and H-C-O bending modes of the hydroxymethyl group. And the band at 960 cm^{-1} can be attributed to the combination of –CO stretching and –CCO deformation modes. The carboxymethylation of inulin was confirmed with the infrared spectra presented on Fig. 1(a). The appearance of bands at 1560 and 1413 cm^{-1} due to anti-symmetric and asymmetric stretching modes of the carboxylate group ($–COO^{–}$) confirms addition of carboxymethyl groups to the inulin polysaccharide chain.[26]

The functionalization of the magnetic nanoparticles with APS and CMI was also confirmed using infrared spectroscopy. Fig. 1(b) shows the infrared spectra of the IO-NPs after modification with APS. The spectra exhibit several bands at 3271, 2924, 1635 and 1315 cm^{-1}. These bands were attributed to –OH stretching, $–CH_2$ stretching, and $-NH_2$ bending modes of free amino groups, respectively.[20] A band characteristic of the attachment of the silane molecule to the iron oxide surface appears at 1006 cm^{-1} and is attributed to Si-O-Et bond formation.[20] When CMI was covalently attached to IO-APS nanoparticles several bands appeared at 1593 and 1313 cm^{-1} that can be assigned to the combination of the –CN stretching and –NH bending of amide II, and to the –CNH stretching of amide III.[26] These bands confirm the amide bond formation between the amine groups of the IO-APS and the carboxylic groups of CMI.

TEM Image Analysis

Fig. 2 shows TEM images and size distribution histograms of IO, IO-APS, and IO-CMI. The TEM images demonstrate that the nanoparticles obtained are rather polydisperse. The average diameter of the primary particles was determined by fitting the size distribution histograms to a lognormal distribution, resulting in mean diameter and geometric deviation values of 11.5 nm and 0.5 for IO, 12.0 nm and 0.4 for IO-APS, and 11.9 nm and 0.4 for IO-CMI. The similarity among these values demonstrates that the nanoparticle core size and shape are not affected by the various modification steps in the synthesis of IO-CMI nanoparticles.

Dynamic Light Scattering and ζ-Potential

The use of IO-CMI nanoparticles for biomedical/biological applications requires demonstration of their colloidal stability under different conditions of ionic strength, pH, temperature, and in cell culture media. We first tested the stability of the particles in water at different NaCl concentrations, pH, and temperatures. The average hydrodynamic diameters (D_h) obtained by DLS are shown in Figure 3. Figure 3(a) shows the hydrodynamic diameter of the IO-CMI nanoparticles suspended in different NaCl concentrations below and above 0.15 M, which is representative of the salt concentration found in many biological fluids. As can be observed the average hydrodynamic diameter fluctuates around 70 ± 10 nm for all the NaCl concentrations studied. Colloidal stability was also tested in solutions at pH 2, 4, 7, 9 and 11, which resulted on average D_h, with the results shown in Figure 3(b). Colloidal stability was also studied at various temperatures from 25 to 60°C. Figure 3(d) shows that the average hydrodynamic diameter remains unchanged at around 60 ± 11 nm, demonstrating that temperature does not significantly affect the stability of the particles.

To confirm the modification of the magnetic nanoparticles with APS and CMI we measured the ζ-potential of the modified nanoparticles at different pH, as shown in Fig. 4. This figure shows that IO-APS nanoparticles have a positive ζ-potential from pH 2 through 9, due to amine groups being protonated and an isoelectric point of ~10. After functionalization of nanoparticles with CMI, a negative ζ-potential is observed from pH 2.5 to 11, due to de-protonation of carboxymethyl groups. The isoelectric point of IO-CMI nanoparticles was ~2.5. The change of ζ-potential of IO-APS from positive to negative after modification with

CMI demonstrates the successful modification of the particles with the polysaccharide. In addition, the ζ-potential of IO-CMI nanoparticles between pH 2.5 and 11 is above −30 mV, hence surface charge contributes to colloidal stability in these nanoparticles.

Superconducting Quantum Interference Device Measurements

Magnetic measurements were performed on powder samples before and after modification with CMI. Fig. 5 shows the field dependent magnetization curves for IO-APS and IO-CMI. Both graphs show a sigmoidal shape with zero coercivity that is characteristic of superparamagnetic materials. However, the saturation magnetization was clearly affected by modification of the nanoparticles with APS and CMI. The value of saturation magnetization for IO-APS was 73 emu/g, while for IO-CMI the value was 31 emu/g. Both values were below the expected value of 96 emu/g for iron oxide. The magnetic diameter of the nanoparticles was calculated by fitting the results in Fig. 5 to the Langevin function weighted by a lognormal particle size distribution. This resulted in a magnetic diameter of 9.9 ± 0.5 nm for IO-APS and 9.8 ± 0.5 nm for IO-CMI. The similarity of these values demonstrates that the magnetic size of the particles was not affected by functionalization. These magnetic diameters are slightly smaller than the values obtained by TEM. This difference is a common occurrence in IO-NPs and has been attributed to a surface layer which does not contribute to the net magnetic moment of the particles.[27]

Specific Absorption Rate Results

The capacity of IO-NPs to dissipate the energy of an applied alternating magnetic field is commonly quantified through the so-called specific absorption rate (SAR). SAR values were determined by measuring the initial rate of temperature rise upon application of the field, and were calculated according to

$$SAR = C_p \frac{m_{solvent}}{m_{IO}} \left. \frac{dT}{dt} \right|_{t=0} \quad (1)$$

where C_p is the specific heat capacity of water (4.18 J/g°C), $m_{solvent}$ is the total mass water, m_{IO} is the total mass of iron oxide nanoparticles, and $dT/dt|_{t=0}$ is the initial rate of temperature rise.

Fig. 6 shows representative results from these experiments, wherein a linear rise in temperature with time is observed. The SAR values at a frequency of 233 kHz and at field amplitudes of 20, 38 and 48 kA/m were 58, 107 and 176 W/g, respectively. These values are higher in comparison to poly(ethylene oxide) coated magnetic nanoparticles of 50–100 nm, for which SAR values were 2 – 13 W/g, measured using 10 kA/m and frequency of 108 kHz.[28] Our values are also comparable with IO nanoparticles from 4 to 35 nm modified with sugars such as rhamnose, mannose, and ribose that resulted in SAR values from 0 to 185 W/g at 21 kA/m and a frequency of 168 kHz;[29] and with glycine passivated IO nanoparticles synthesized by co-precipitation having a primary nanoparticle diameter of 10 nm (D_h ~ 30 nm) that resulted in a SAR value of 54.9 W/g at a concentration of 6 mg/mL and at 250 kHz and 18.5 kA/m.[30]

Colloidal Stability of IO-CMI over prolonged periods

The long term colloidal stability of the IO-CMI nanoparticles was tested in water, PBS, 0.15 M NaCl and pH 7. All measurements were performed at room temperature (25°C) and at a representative physiological temperature (37°C) to observe if there were differences in colloidal stability under these conditions. Fig. 7(a) shows that the average hydrodynamic diameter of these particles decreased from around 70 nm to around 40 nm when suspended

in water at 25°C and 37°C for 28 days. The slow decrease in the hydrodynamic diameter of the particles may be due to precipitation of larger nanoparticles over time. Similar behavior was observed in pH 7 at 25°C and 37 °C during the 20 days observed (Fig. 7(d)). However, in 0.15 M NaCl the IO-CMI nanoparticles showed a stable hydrodynamic diameter at around 50 nm at both temperatures. In contrast, when the IO-CMI nanoparticles were suspended in PBS precipitation was observed after three days at 25°C and after 12 to 24 hours at 37 °C. It is interesting that studies in NaCl and at various pH in KNO_3 solutions suggest that the nanoparticles are stabilized sterically, but experiments in PBS demonstrate loss of stability. Agglomeration of other nanoparticles, such as, titanium oxide, zinc oxide, silicon oxide, single-walled carbon nanotubes, and multi-walled carbon nanotubes in PBS has also been observed.[31] PBS is a mixture of 0.01 M of phosphate salts, 0.138 M NaCl, and 0.0027 M of KCl at pH 7.4. Loss of colloidal stability of magnetic nanoparticles in PBS has been attributed to preferential adsorption of phosphate ions on the surface of iron oxide nanoparticles, causing displacement of coatings used to stabilize the particles.[32, 33] However, because here the CMI is covalently grafted to the particles through the APS layer, displacement of CMI by phosphate ions would seem unlikely. Indeed, IO-CMI particles suspended in 0.01 M solution of potassium phosphate at pH 7.4 in the absence of NaCl or KCl were stable for 7 days at 25 °C and 37 °C. This would seem to indicate that loss of stability in PBS is through another, as yet undetermined, mechanism.

Colloidal Stability of IO-CMI in Cell Culture Media

Due to the unexpected colloidal instability of the IO-CMI nanoparticles in PBS, we studied the effect of culture medium prior to any *in vitro* or *in vivo* experiments. Fig. 8 shows the average D_h as a function of time for IO-CMI nanoparticles in DMEM, EMEM and RPMI culture media. These experiments were performed at 25°C and 37°C.

The experiments showed that for IO-CMI nanoparticles suspended in DMEM, Fig. 8(a–b), at 25°C the particles precipitate after 12 hours in the absence of FBS but remain suspended for 48 hours in the presence of FBS. At 37°C the IO-CMI nanoparticles suspended in DMEM without FBS were only stable for 6 hours but with FBS in solution the particles remained suspended for 48 hours. Fig. 8(a–b) also revealed that with FBS at 25°C and 37°C the hydrodynamic diameter of the particles first increases, then reaches a maximum between 12 and 24 hours, and then starts to decrease. This behavior could imply that the particles first aggregate and then precipitate after reaching a maximum size. This behavior was not observed for particles suspended in DMEM without FBS where the hydrodynamic diameter increased over time and then the particles rapidly precipitated.

The behavior of the IO-CMI nanoparticles suspended in EMEM was similar to that observed in DMEM. Fig. 8(c) demonstrates that at 25°C the particles suspended in EMEM without FBS were stable for 12 hours. However, with FBS at that same temperature the particles were stable for 24 hours and under the same conditions with DMEM the particles remained suspended for at least 48 hours. At 37 °C the nanoparticles in EMEM without FBS agglomerated rapidly and after 6 hours all the particles had precipitated (see Fig. 8(d)). When FBS was present in solution the nanoparticles remained suspended for 48 hours but their size increased significantly.

Fig. 8(e) shows the average hydrodynamic diameter of the IO-CMI nanoparticles suspended in RPMI with and without FBS at 25°C. As can be observed, without FBS the particles remained stable for 24 hours and with FBS they remained stable for 72 hours. When the particles were exposed to RPMI without FBS at 37°C the time in suspension was only 6 hours. When FBS was present the particles remained in suspension for 72 hours and were slightly smaller than observed at 25°C.

In general, the stability of the IO-CMI nanoparticles improved upon addition of FBS. This is probably due to adsorption of proteins in FBS to the nanoparticles. Higher stability in cell culture media with proteins has been observed before with magnetic nanoparticles coated with different molecules such as dextran, polyarabic acid, sodium phosphate, and polyvinyl alcohol.[34] However, in those cases the particles were found to be stable for much shorter times of 19 to 60 minutes. Proteins such as albumin in culture media can have a significant role in preventing or slowing down agglomeration on a wide variety of metal, metal oxides and carbonaceous materials.[31, 35–37] Ji and collaborators found that divalent cations such as Ca^{2+} in the cell culture medium can bridge negatively charged nanoparticles and proteins in FBS, contributing to loss of stability.[38] It is interesting to note that in those studies the bare particles were stabilized by electrostatic interactions with negatively charged surfaces, thus the higher ionic strength in a culture medium would lead to loss of stability and agglomeration, whereas the presence of divalent cations and proteins leads to formation of a protein coating which confers steric stabilization. In the case of the studies reported here, our experiments in NaCl and phosphate ion solutions, and at various pH in deionized water adjusted with potassium nitrate support a steric mechanism of colloidal stabilization in the IO-CMI particles. Hence, we surmise that the loss of colloidal stability in PBS and other culture media is due to a mechanism besides charge screening due to the higher ionic strength. It would seem that in our case, in the absence of proteins the presence of divalent cations leads to bridging between particles and particle agglomeration. When FBS is added, the divalent cations lead to bridging of particles and proteins, leading to slower aggregation and precipitation. In any case, in the presence of proteins the particles are found to be colloidally stable at room temperature and at physiologic temperature for periods of up to 72 hours, which may make them suitable for biomedical applications.

Cytotoxicity

The cytotoxicity of IO-CMI nanoparticles toward five common cancer cell lines was tested. Fig. 9 shows the viability of A2780, Caco-2, Hey A8 FDR, MCF-7 and MDA-MB-468 cells exposed to different concentrations of IO-CMI nanoparticles. As can be observed in Fig. 9(a) A2780 cells were most susceptible to the IO-CMI nanoparticles, followed by Hey A8 FDR and MDA-MB-468. For A2780 cells, IO-CMI resulted in a statistically significant decrease in cell viability for concentrations of IO-CMI above 0.1 mg/ml. For Caco-2 and MCF-7 cell lines, Fig. 8(b) and 8(d), a statistically significant decrease in cell viability was only observed at the highest concentration of IO-CMI nanoparticles (3.5 mg/mL).

In the past our group has tested the effect on cell viability of iron oxide nanoparticles covered with carboxymethyl-dextran (IO-CMDx).[39] In summary, for IO-CMDx we have observed a decrease in cell viability to ~80% at a concentration of 0.90 mg/mL for Caco-2 and MCF-7 cell lines. In comparison, at a concentration of 1.5 mg/mL IO-CMI the nanoparticles resulted in cell viabilities of 90 % and 96 % in Caco-2 and MCF-7 cell lines, respectively. This indicates that IO-CMI nanoparticles are not significantly toxic to any of the cell lines tested, even though there seem to be some differences in cell response to the particles. When we compare the of IO-CMI on cell viability in Caco-2 with other nanoparticles reported in the literature we found that they are less toxic even when higher concentration (1.5 mg/mL) were used in our experiments. For example, 10 μg/mL of peptide coated 40 nm silver nanoparticles nm were found to lower cell viability to 60% after 48 hours in Caco-2 cells.[40] Single-walled carbon nanotubes functionalized with carboxylic acid have been found to be toxic to Caco-2 cells above 100 μg/mL.[41] As with Caco-2 cells, our IO-CMI nanoparticles are less toxic than other nanoparticles in the cell line MCF-7. Silica nanoparticles of approximately 100 nm size without any modification were found to lower cell viability to less than 80 % after 24 hours in contact with MCF-7 cells using a concentration of less than 10 μg/mL.[42] Iron oxide nanoparticles of approximately 40 nm

coated with poly(ethylenimine) lowered cell viability to less than 80 % in MCF-7 after 24 hr exposure at 0.25 μg/mL.[43]

Uptake of IO-CMI by Caco-2 cells

Caco-2 cells were exposed to 100 μg of total iron (according to the 1,4-phenanthroline assay[22]) for 1, 6, 12 and 24 hours. As can be observed in Fig. 10(a), iron content per cell increased over time, indicating an increase in uptake of the IO-CMI nanoparticles. To determine the effect of IO-CMI nanoparticle concentration on uptake by Caco-2 cells, several suspensions were prepared with 20, 40, 60, 80 and 100 μg of total iron and incubated with cells for a period of 24 hours. Fig. 10(b) shows that an increase in IO-CMI nanoparticle concentration resulted in an increase in the iron content per cell.

Pharmacokinetic Study

Fig. 11 shows the average plasma Fe content as a function of time. Immediately after nanoparticle injection the Fe concentration is found to be higher than the baseline Fe concentration. Subsequently the Fe concentration decays monotonically, apparently following exponential decay. We ascribe this to initial delivery of the iron oxide nanoparticles and their subsequent clearance. We note that at prolonged times the plasma Fe content remains significantly higher than the initial baseline, which we attribute to hemolysis occurring during sample extraction. In order to estimate the circulation time of the IO-CMI nanoparticles in the blood we fitted the plasma Fe concentration to an exponential decay model,

$$c\,[\mathrm{ug\ Fe}/g\ \mathrm{plasma}]=c_{\infty}+c^{*}\exp\left(-\frac{t}{\tau}\right), \quad (2)$$

resulting in a time constant τ of 47±3 min.

Conclusions

We have demonstrated the use of carboxy-methyl inulin (CMI) as a biocompatible coating for iron oxide nanoparticles which confers colloidal stability over a biomedically relevant time window of ~24–72 hr, depending on the make-up of the suspension medium. The CMI was covalently grafted to the iron oxide (IO) nanoparticles by first condensing an amine-silane on the IO surface, leaving amine groups exposed at the surface. Then, those groups were used to modify the surface with CMI via amide bond formation. The step-by-step functionalization of the nanoparticles was followed using dynamic light scattering. An increase in hydrodynamic diameter, from 42 nm for IO-APS to 55 nm for IO-CMI, was attributed to the attachment of CMI to the nanoparticles. The FT-IR results of IO-APS shows the characteristic vibrational modes for the amine and siloxane groups while the spectra of IO-CMI shows the fructose and the amide vibrational modes that confirm the CMI attachment to the IO-APS nanoparticles. Furthermore, zeta potential measurements at different pH's showed a positive potential from pH 2 through 9 for IO-APS due to amine group protonation, and an isoelectric point at around 9.8. Meanwhile, CMI functionalized nanoparticles showed a negative zeta potential from pH 2.5 through 11 due to the de-protonation of the carboxylic acid group. The IO core size distribution of the particles was around 11 nm for each step of the synthesis, which suggests that the larger hydrodynamic diameter of the particles arose from the formation of clusters that can be observed in the TEM images. The IO core diameters determined from TEM were in agreement with the magnetic core diameter obtained by fitting magnetization measurements to the Langevin function. Our results demonstrate that the IO-CMI particles maintain their hydrodynamic diameter in NaCl at concentrations under and above the physiological concentrations (150

mM NaCl) as well as at a pH range from 2 to 11 and at temperatures between 25°C and 60°C. The IO-CMI nanoparticles were stable with time after being stored in water, potassium phosphate monobasic solution at pH 7.4 and cell culture medium (DMEM, EMEM and RPMI with FBS). IO-CMI nanoparticle cytotoxicity experiments were conducted in ovarian, breast and colon cancer cell lines. Those experiments have demonstrated satisfactory cell viability. Uptake studies were conducted using Caco-2 as a model cell line to demonstrate that these nanoparticles can be internalized by cells. Observations of IO-CMI blood circulation time show elimination of the nanoparticles from the bloodstream, with a characteristic time constant of 47±3 min. In summary, the results presented here suggest that these particles can be further used for *in vitro* and *in vivo* studies to establish their potential in biomedical applications.

Acknowledgments

We are grateful to Belisa Suarez for assistance in conducting the pharmacokinetics study, to Roberto Olayo-Valles for TEM experiments, and to Felix Roman for access to the ICP-MS instrument. This project was supported by the US National Institutes of Health (1 R15 EB010228-01) and the US National Science Foundation (EPS-1002410).

Notes and references

1. Laurent S, Forge D, Port M, Roch A, Robic C, Vander Elst L, Muller RN. Magnetic Iron Oxide Nanoparticles: Synthesis, Stabilization, Vectorization, Physicochemical Characterizations, and Biological Applications. Chemical Reviews. 2008; 108(6):2064–2110. [PubMed: 18543879]
2. Shubayev VI, Pisanic TR II, Jin S. Magnetic nanoparticles for theragnostics. Advanced Drug Delivery Reviews. 2009; 61(6):467–477. [PubMed: 19389434]
3. Pankhurst QA, Connolly J, Jones SK, Dobson J. Applications of magnetic nanoparticles in biomedicine. Journal of Physics D-Applied Physics. 2003; 36(13):R167–R181.
4. Pankhurst QA, Thanh NTK, Jones SK, Dobson J. Progress in applications of magnetic nanoparticles in biomedicine. Journal of Physics D-Applied Physics. 2009; 42(22)
5. Wu W, He Q, Jiang C. Magnetic Iron Oxide Nanoparticles: Synthesis and Surface Functionalization Strategies. Nanoscale Research Letters. 2008; 3(11):397–415. [PubMed: 21749733]
6. Choi HS, Liu W, Misra P, Tanaka E, Zimmer JP, Ipe BI, Bawendi MG, Frangioni JV. Renal clearance of quantum dots. Nature Biotechnology. 2007; 25(10):1165–1170.
7. Gunatillake PA, Adhikari R. Biodegradable synthetic polymers for tissue engineering. Eur Cell Mater. 2003; 5:1–16. discussion 16. [PubMed: 14562275]
8. Wang X, Ishida T, Kiwada H. Anti-PEG IgM elicited by injection of liposomes is involved in the enhanced blood clearance of a subsequent dose of PEGylated liposomes. Journal of Controlled Release. 2007; 119(2):236–244. [PubMed: 17399838]
9. Dias AMGC, Hussain A, Marcos AS, Roque ACA. A biotechnological perspective on the application of iron oxide magnetic colloids modified with polysaccharides. Biotechnology Advances. 2011; 29(1):142–155. [PubMed: 20959138]
10. Amstad E, Textor M, Reimhult E. Stabilization and functionalization of iron oxide nanoparticles for biomedical applications. Nanoscale. 2011; 3(7):2819–2843. [PubMed: 21629911]
11. Newcombe R. Precautions in the intravenous use of iron-dextran. Postgrad Med J. 1967; 43(499): 372–5. [PubMed: 6042393]
12. Wheatley MA, Moo-Young M. Degradation of polysaccharides by endo- and exoenzymes: Dextran–dextranase model systems. Biotechnology and Bioengineering. 1977; 19(2):219–233. [PubMed: 856322]
13. Barclay T, Ginic-Markovic M, Cooper P, Petrovsky N. Inulin - a versatible polysaccharide with multiple pharmaceutical and food chemical uses. J Excipients and Food Chem. 2010; 1(3):27–50.
14. Van Loo J, Coussement P, De Leenheer L, Hoebregs H, Smits G. On the presence of Inulin and Oligofructose as natural ingredients in the western diet. Critical Reviews in Food Science and Nutrition. 1995; 35(6):525–552. [PubMed: 8777017]

15. Stevens CV, Meriggi A, Booten K. Chemical Modification of Inulin, a Valuable Renewable Resource, and Its Industrial Applications. Biomacromolecules. 2001; 2(1):1–16. [PubMed: 11749147]
16. Reddy BS, Hamid R, Rao CV. Effect of dietary oligofructose and inulin on colonic preneoplastic aberrant crypt foci inhibition. Carcinogenesis. 1997; 18(7):1371–1374. [PubMed: 9230282]
17. Jung K, Henke W, Schulze BD, Sydow K, Precht K, Klotzek S. Practical approach for determining glomerular filtration rate by single-injection inulin clearance. Clinical Chemistry. 1992; 38(3): 403–7. [PubMed: 1547559]
18. Verraest DL, Peters JA, Batelaan JG, van Bekkum H. Carboxymethylation of inulin. Carbohydrate Research. 1995; 271(1):101–112. [PubMed: 7648576]
19. Johannsen FR. Toxicological profile of carboxymethyl inulin. Food and Chemical Toxicology. 2003; 41(1):49–59. [PubMed: 12453728]
20. Herrera AP, Barrera C, Rinaldi C. Synthesis and functionalization of magnetite nanoparticles with aminopropylsilane and carboxymethyldextran. Journal of Materials Chemistry. 2008; 18(31): 3650–3654.
21. Creixell M, Herrera AP, Ayala V, Latorre-Esteves M, Pérez-Torres M, Torres-Lugo M, Rinaldi C. Preparation of epidermal growth factor (EGF) conjugated iron oxide nanoparticles and their internalization into colon cancer cells. Journal of Magnetism and Magnetic Materials. 2010; 322(15):2244–2250.
22. ASTM. Standard test method for iron in trace quantities using 110-phenanthroline method. ASTM E394-00. 2000
23. Bernal BH, Calle J, Duarte EQ, Pinzon R, Velazquez M. Inulin from tubers of *Dahlia imperialis* Roetz. Rev Col Cienc Quim Farm. 2005; 34(2):122–125.
24. Ibrahim M, Alaam M, El-Haes H, Jalbout AF, Leon Ad. Analysis of the structure and vibrational spectra of glucose and fructose. Eclética Química. 2006; 31:15–21.
25. Szarek WA, Korppi-Tommola S-L, Shurvell HF, Smith VH Jr, Martin ORA. Raman infrared study of crystalline D-fructose L-sorbose, related carbohydrates Hydrogen bonding and sweetness. Canadian Journal of Chemistry. 1984; 62(8):1512–1518.
26. Smith, AL. Applied Infrared Spectroscopy. John Wiley and Sons; New York: 1979.
27. Gupta M, Sharma M. Aggregation behavior of iron oxide nanoparticles measured by SQUID magnetometry. International Journal of Nanoscience. 2011; 10(04n05):647–651.
28. Aqil A, Vasseur S, Duguet E, Passirani C, Benoît JP, Roch A, Müller R, Jérôme R, Jérôme C. PEO coated magnetic nanoparticles for biomedical application. European Polymer Journal. 2008; 44(10):3191–3199.
29. Lartigue L, Innocenti C, Kalaivani T, Awwad A, Sanchez Duque MdM, Guari Y, Larionova J, Guérin C, Montero J-LG, Barragan-Montero V, Arosio P, Lascialfari A, Gatteschi D, Sangregorio C. Water-Dispersible Sugar-Coated Iron Oxide Nanoparticles An Evaluation of their Relaxometric and Magnetic Hyperthermia Properties. Journal of the American Chemical Society. 2011; 133(27): 10459–10472. [PubMed: 21604803]
30. Barick KC, Hassan PA. Glycine passivated Fe3O4 nanoparticles for thermal therapy. Journal of Colloid and Interface Science. 2012; 369(1):96–102. [PubMed: 22209576]
31. Bihari P, Vippola M, Schultes S, Praetner M, Khandoga A, Reichel C, Coester C, Tuomi T, Rehberg M, Krombach F. Optimized dispersion of nanoparticles for biological in vitro and in vivo studies. Particle and Fibre Toxicology. 2008; 5(1):14. [PubMed: 18990217]
32. Miles WC, Goff JD, Huffstetler PP, Reinholz CM, Pothayee N, Caba BL, Boyd JS, Davis RM, Riffle JS. Synthesis and colloidal properties of polyether magnetite complexes in water and phosphate-buffered saline. Langmuir. 2009; 25(2):803–813. [PubMed: 19105718]
33. Creixell M, Herrera AP, Latorre-Esteves M, Ayala V, Torres-Lugo M, Rinaldi C. The effect of grafting method on the colloidal stability and in vitro cytotoxicity of carboxymethyl dextran coated magnetic nanoparticles. Journal of Materials Chemistry. 2010; 20(39):8539–8547.
34. Eberbeck D, Kettering M, Bergemann C, Zirpel P, Hilger I, Trahms L. Quantification of the aggregation of magnetic nanoparticles with different polymeric coatings in cell culture medium. Journal of Physics D-Applied Physics. 2010; 43(40)

35. Chanteau B, Fresnais J, Berret JF. Electrosteric Enhanced Stability of Functional Sub-10 nm Cerium and Iron Oxide Particles in Cell Culture Medium. Langmuir. 2009; 25(16):9064–9070. [PubMed: 19572532]

36. Murdock RC, Braydich-Stolle L, Schrand AM, Schlager JJ, Hussain SM. Characterization of Nanomaterial Dispersion in Solution Prior to In Vitro Exposure Using Dynamic Light Scattering Technique. Toxicological Sciences. 2008; 101(2):239–253. [PubMed: 17872897]

37. Zook JM, Maccuspie RI, Locascio LE, Halter MD, Elliott JT. Stable nanoparticle aggregates/agglomerates of different sizes and the effect of their size on hemolytic cytotoxicity. Nanotoxicology. 2011; 5(4):517–30. [PubMed: 21142841]

38. Ji Z, Jin X, George S, Xia T, Meng H, Wang X, Suarez E, Zhang H, Hoek EMV, Godwin H, Nel AE, Zink JI. Dispersion and Stability Optimization of TiO2 Nanoparticles in Cell Culture Media. Environmental Science & Technology. 2010; 44(19):7309–7314. [PubMed: 20536146]

39. Rodriguez-Luccioni HL, Latorre-Esteves M, Mendez-Vega J, Soto O, Rodriguez AR, Rinaldi C, Torres-Lugo M. Enhanced reduction in cell viability by hyperthermia induced by magnetic nanoparticles. Int J Nanomedicine. 2011; 6:373–80. [PubMed: 21499427]

40. Böhmert L, Niemann B, Thünemann A, Lampen A. Cytotoxicity of peptide-coated silver nanoparticles on the human intestinal cell line Caco-2. Archives of Toxicology. 2012; 86(7):1107–1115. [PubMed: 22418598]

41. Jos A, Pichardo S, Puerto M, Sánchez E, Grilo A, Cameán AM. Cytotoxicity of carboxylic acid functionalized single wall carbon nanotubes on the human intestinal cell line Caco-2. Toxicology in Vitro. 2009; 23(8):1491–1496. [PubMed: 19591917]

42. Lebret V, Raehm L, Durand J-O, Smaïhi M, Werts MV, Blanchard-Desce M, Méthy-Gonnod D, Dubernet C. Surface functionalization of two-photon dye-doped mesoporous silica nanoparticles with folic acid: cytotoxicity studies with HeLa and MCF-7 cancer cells. Journal of Sol-Gel Science and Technology. 2008; 48(1–2):32–39.

43. Hoskins C, Cuschieri A, Wang L. The cytotoxicity of polycationic iron oxide nanoparticles: Common endpoint assays and alternative approaches for improved understanding of cellular response mechanism. Journal of Nanobiotechnology. 2012; 10(1):15. [PubMed: 22510488]

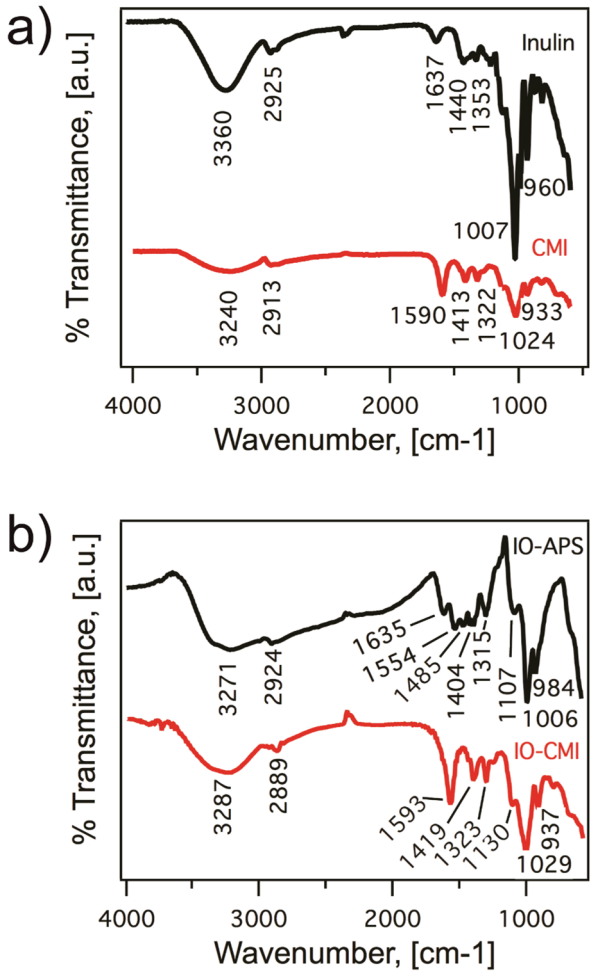

Fig. 1.
FT-IR spectra of (a) inulin and CMI, and (b) IO-APS and IO-CMI.

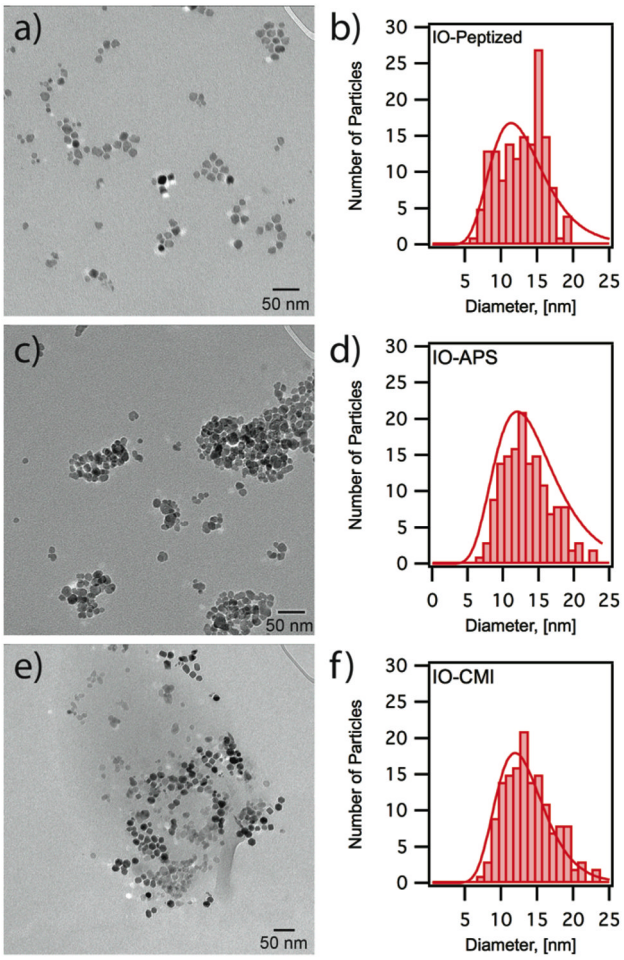

Fig. 2.

TEM images and size distribution histograms of bare IO (a and b), IO-APS (c and d) and IO-CMI (e and f) nanoparticles.

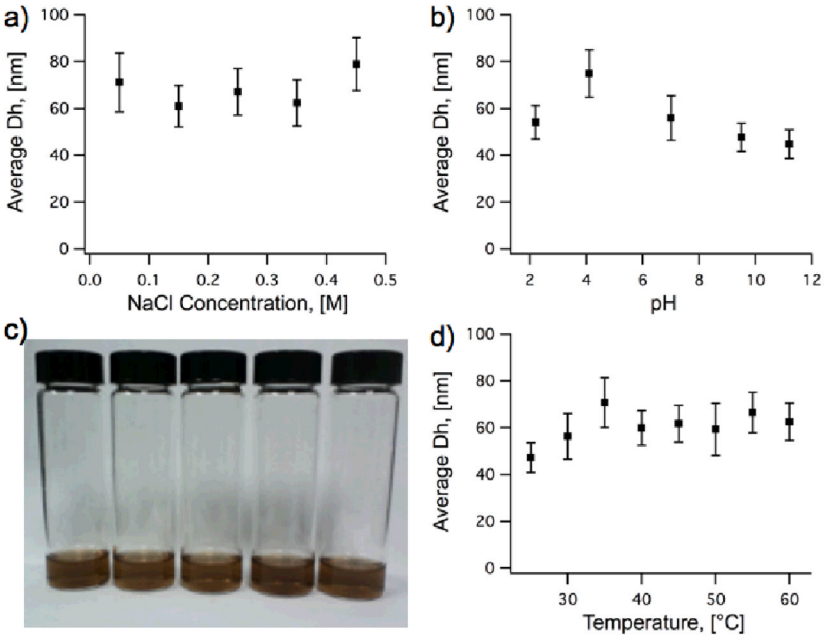

Fig. 3.

Hydrodynamic diameter of IO-CMI nanoparticles at different a) and c) NaCl concentrations, b) pH and d) temperatures.

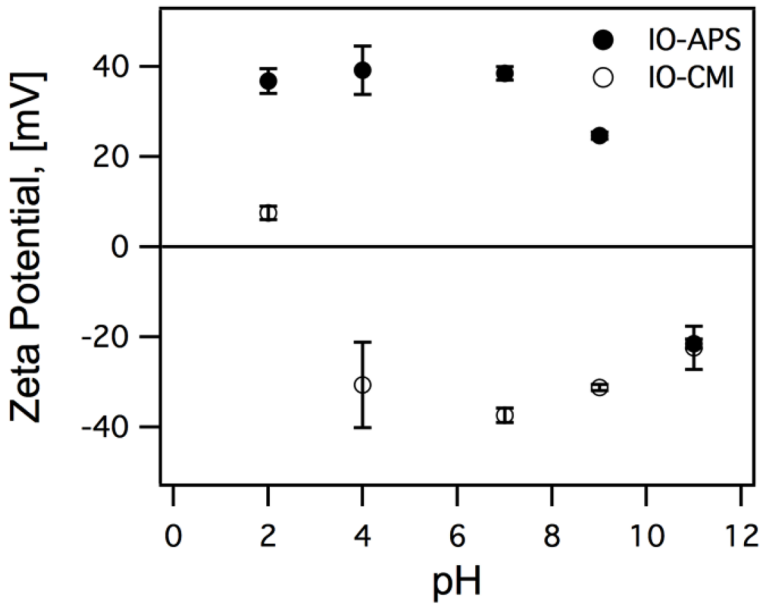

Fig. 4.
Plot of ζ-potential vs pH of IO-APS and IO-CMI.

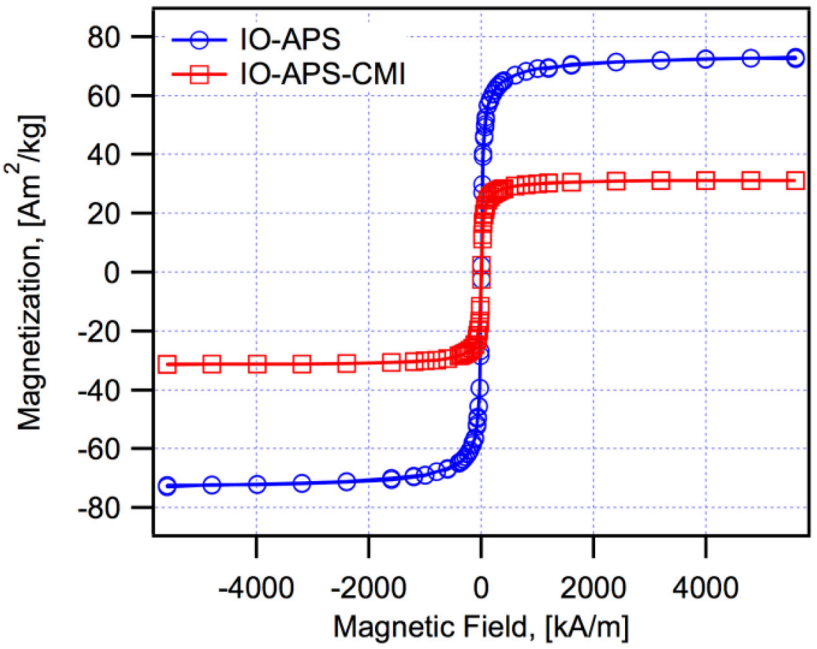

Fig. 5.
Field dependence of magnetization at 300 K for IO-APS and IO-CMI nanoparticles.

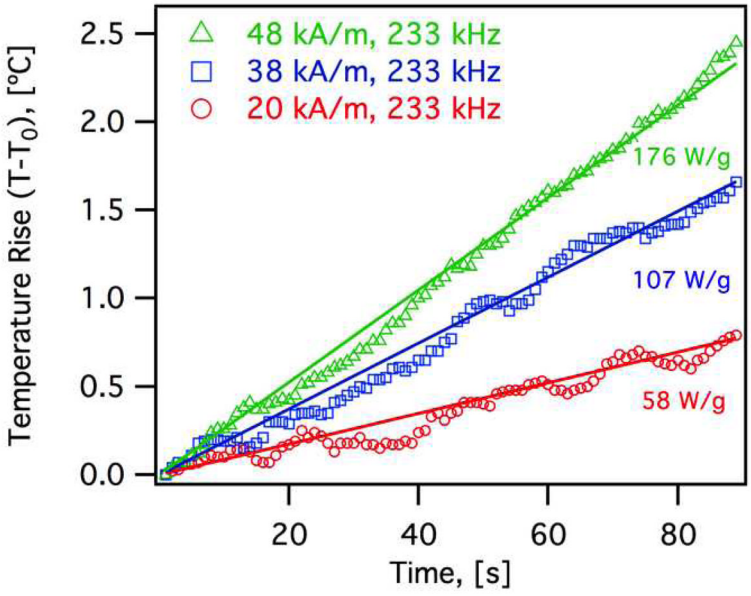

Fig. 6.

Temperature rise for IO-CMI nanoparticles subjected to alternating magnetic fields of various amplitudes.

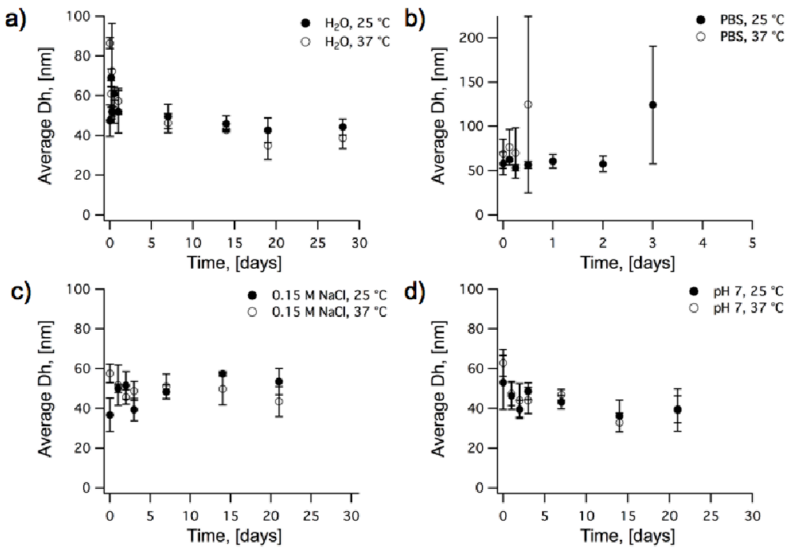

Fig. 7.

Colloidal stability of IO-CMI nanoparticles after incubation in (a) deionized water, (b) PBS, (c) 0.15 M NaCl at pH 7, and (d) deionized water with pH adjusted to 7, all at 25°C and 37°C.

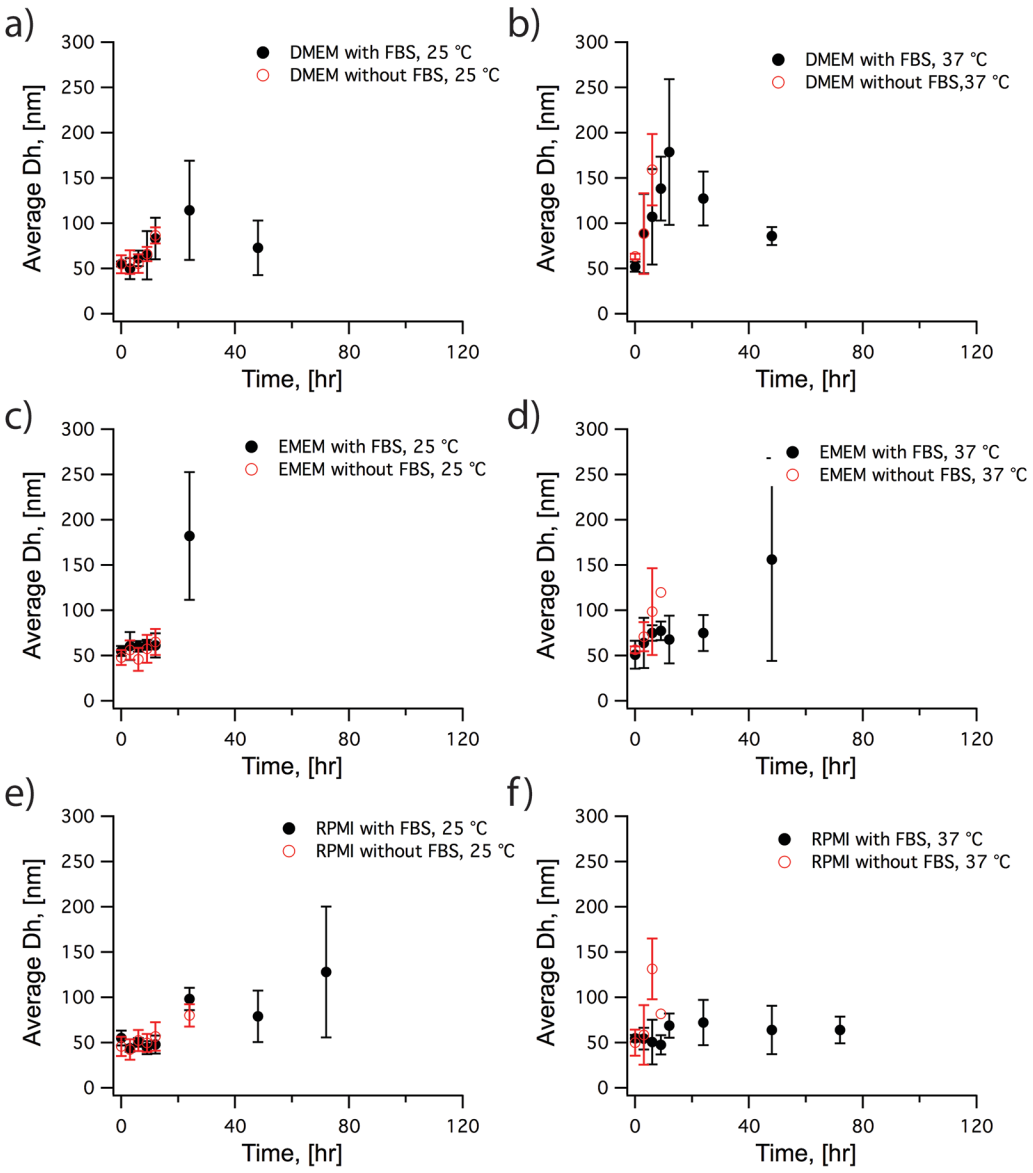

Fig. 8.

Colloidal Stability of IO-CMI nanoparticles in (a,b) DMEM, (c,d) EMEM and (e,f) RPMI with and without FBS at 25°C and 37°C

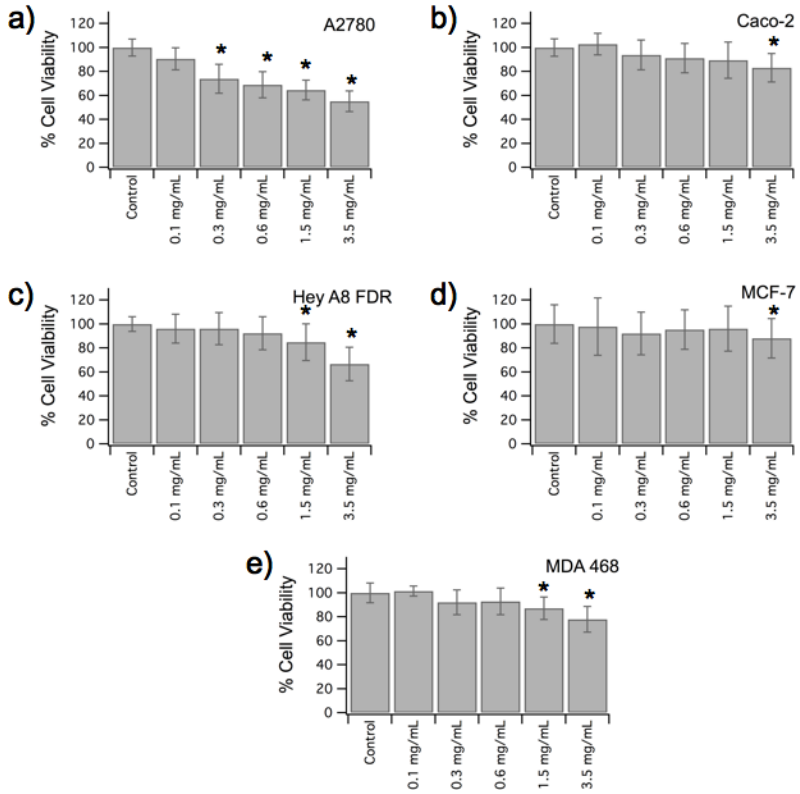

Fig. 9.

Effect of incubation with IO-CMI nanoparticles at various concentrations (0.1, 0.3, 0.6, 1.5 and 3.5 mg/mL) on cell viability of (a) A2780, (b) Caco-2, (c) Hey A8 FDR, (d) MCF-7 and (e) MDA-MB-468 cell lines. Each value is expressed as mean ± RSD (n=37, *$p < 0.05$).

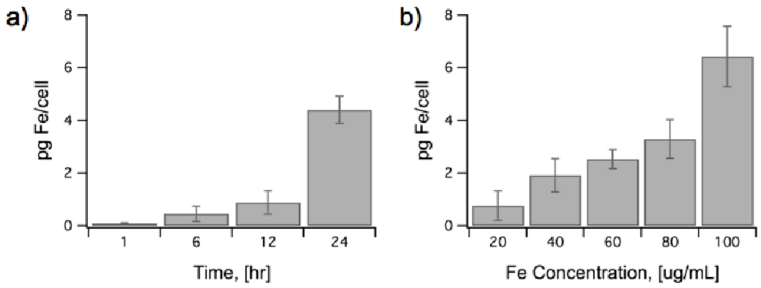

Fig. 10.

(a) Uptake of 100 ug/mL of IO-CMI nanoparticles after 1,6, 12 and 24 hours of exposure to Caco-2 cells. (b) Internalization of different concentrations (20, 40, 60, 80, and 100 ug/mL) of IO-CMI nanoparticles in Caco-2 cells after exposure for 24 hours.

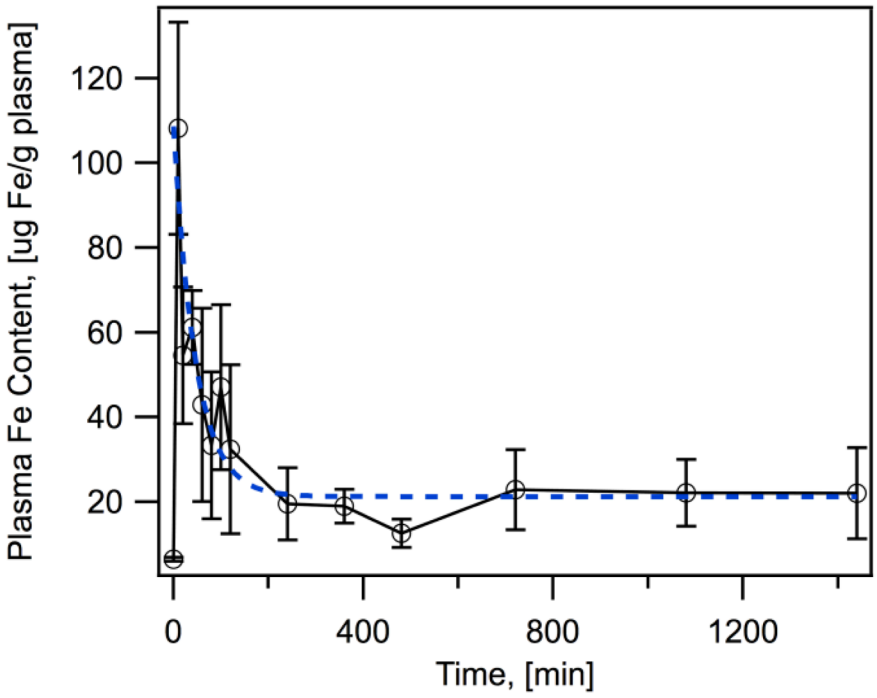

Fig. 11.

Average plasma Fe content as a function of time. Error bars correspond to the standard deviation of the measurements for five animals. The dashed line corresponds to an exponential fit to the data spanning 10 to 1440 min.